Measuring the diffusion of fluorescent dye or protein inside living cells

Saumya Prasad and Rajaram Swaminathan*

Department of Biotechnology, Indian Institute of Technology Guwahati, Guwahati 781 039, India

Information about the space and time inside a living cell is important to fully understand the different molecular events that occur in the cell. The cell cytoplasm, interior of a red blood cell or mitochondrial matrix are spaces crowded with macromolecules like proteins, for example. What are the consequences of such molecular crowding on the rate of transport of solutes or metabolites within the cell is not clear. Is diffusion alone sufficient to take small solutes to different corners of the cell? Fluorescence microscopy provides a non-invasive approach to understand the inner workings of a living cell. Techniques like fluorescence recovery after photobleaching and time-resolved fluorescence anisotropy have made it possible to observe diffusion of small dyes like BCECF and average size proteins like GFP inside living cells in real time. In this article, we introduce fluorescence microscopy, its advantages/limitations and briefly highlight a few observations of diffusion inside living cells.

Keywords: Diffusion, fluorescence anisotropy, green fluorescent protein, photobleaching, total internal reflection fluorescence.

A LARGE store selling high-value items like jewellery is constantly monitored by surveillance cameras placed at strategic locations to instantly detect theft of goods or any such suspicious behaviour. Live video feeds from such cameras projected on a monitor can instantly alert a person in the security control room on an abnormal activity occurring at any chosen site in the store.

The onset of disease in a living cell is also triggered by abnormal events inside the cell which often occur well before disease phenotype, in the form of symptoms that are diagnosed. So it would be useful to track abnormal molecular events inside a cell to anticipate arrival of disease. Unfortunately such a task is made difficult by the hierarchy of scales involved. Unlike the goods and thieves in the store, the elements inside the cell, namely subcellular organelles, proteins, cytoskeleton and metabolites, exist in a multitude of sizes ranging from several angstroms to a few microns, making it difficult to see them all. So even though the cell (~ 10 μm) is rendered visible to the naked eye by the magnifying optics of the light microscope, its internal components in the submicrometre dimension are barely resolved owing to the Abbe diffraction limit[1,2], which has been overcome[3] and given rise to super-resolution imaging[4,5]. To observe features at the nanometre or sub-nanometre dimension, techniques like transmission electron microscopy (TEM)[6], which use electrons instead of light to impinge on the sample can be employed. However, TEM observations cannot be made on live cells because of the harsh sample preparation procedures that demand ultra-thin (~ nm) sample slices during measurement[7–9]. To monitor events in real time inside living cells, fluorescence microscopy has emerged as the technique of choice[10–13].

What is fluorescence microscopy?

The main purpose of a fluorescence microscope is twofold. First to uniformly illuminate a spot of typically 1–100 μm diameter on the sample (typically a colony of live eukaryotic cells grown on a glass coverslip soaked in cell culture medium or phosphate buffered saline (PBS)), thereby exciting fluorescent molecules (fluorophores) inside the living cell with incident photons. Second, the emitted fluorescence from excited sample fluorophores is promptly collected after filtering out the excitation photons. Figure 1 shows a typical schematic for an epi-fluorescence set-up that is commonly employed in fluorescence microscopy. Such a set-up forms the backbone for techniques like fluorescence correlation spectroscopy (FCS) and fluorescence recovery after photobleaching (FRAP). The versatility of the fluorescence microscopy techniques arises from the multiple ways in which the spatial location of the illumination spot, wavelength, polarization, intensity and temporal properties of the emitted photon can be analysed in response to manipulations in the excitation light source, to gather useful information on the cellular milieu around the excited fluorophore[14–16].

Advantages of using fluorescence microscopy

- Requires negligible energy (< nJ) to electronically excite a fluorophore inside the cells making it harmless and non-invasive.
- Wide repertoire of fluorescent probes[17–25] or quantum dots[26–29] spanning emission wavelengths from ultra-

*For correspondence. (e-mail: rsw@iitg.ernet.in)

violet to near-infrared enables imaging with multiple probes simultaneously, especially with multi-photon excitation.
- State-of-the-art detectors (photomultiplier tubes, avalanche photodiodes) that at best can be sensitive enough to image fluorescence from single molecules[30–34]. This also enables extremely dilute or weakly fluorescent samples to be studied, provided the background is sufficiently dark.
- Up to nanosecond time resolution to monitor dynamic events like diffusion, protein folding and gene expression inside a cell.
- Reduced background fluorescence from endogenous probes inside the cell (autofluorescence) when exciting with $\lambda > 600$ nm.
- Advent of endogenous probes like green fluorescent protein (GFP)[35–39] that can be selectively expressed at chosen spatial locations inside the cell.

Limitations of using fluorescence microscopy

- Limited penetration of single-photon excitation light into tissues like skin[40–43].
- Need for endogenous probes that are smaller in molecular weight ($M_w \ll 30$ kDa) than GFP.

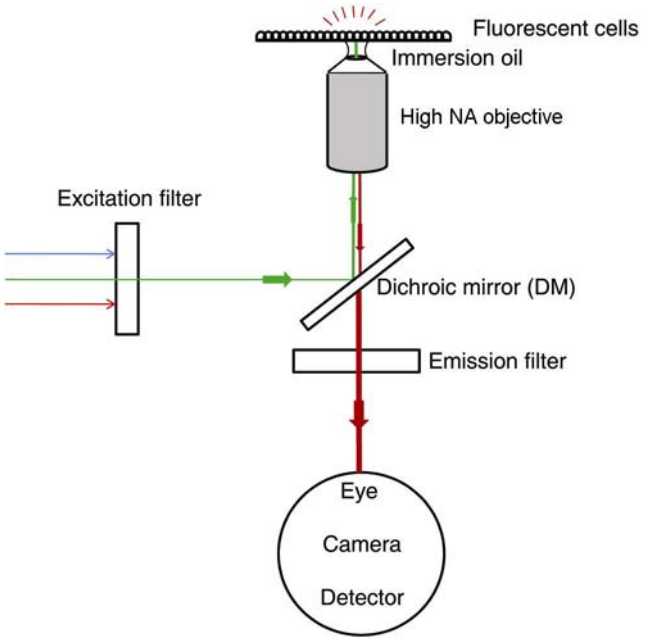

Figure 1. Optical layout in an inverted epifluorescence microscope. The optical paths of excitation (green line) and emission (red line) through the objective are identical in an epifluorescence configuration. They are shown separately here for visual clarity. The excitation filter is redundant if laser beam is the excitation source. The Dichroic mirror transmits the long wavelength fluorescence photons which are further filtered using a long-pass emission filter that blocks excitation photons. In an epifluorescence set-up, the same objective illuminates the sample and also collects emitted fluorescence in identical light paths. A high numerical aperture objective is essential to capture a large fraction of weakly emitted fluorescence.

- Tedious approaches like microinjection or probe derivative design to introduce fluorescent probes inside the living cell and maintain them there as well[44–46].
- Inability to collect all emitted fluorescence photons that can dramatically improve signal/noise in weakly emitting or dilutes samples.
- Scattering of emitted light from dense samples.
- Interference from autofluorescence[47]/quenching, for example, from haemoglobin in blood[48], chlorophyll in leaf[49], FMN, FAD or NADH in cell cytosol[50], lipofuscin in brain tissue, collagen and elastin in connective tissue[51].

Useful fluorescence parameters to monitor from a fluorophore inside a cell

Fluorescence intensity ratio

Measuring the emission intensity of a fluorophore residing inside a living cell does not yield any useful information. The fluorescence intensity at emission wavelength λ is given by:

$$F(\lambda) = \varepsilon(\lambda_{exc})\phi_F f(\lambda) C I_0 K, \quad (1)$$

where $\varepsilon(\lambda_{exc})$ is the molar extinction coefficient of the fluorophore at excitation wavelength, ϕ_F the fluorescence quantum yield, $f(\lambda)$ the fraction of total fluorescence emitted at wavelength λ, C the concentration of fluorophore, I_0 refers to intensity of excitation light and K is a constant that depends on instrumental parameters like light collection efficiency, sample chamber pathlength and other factors.

To begin with this intensity cannot be directly correlated to fluorophore concentration in the excitation volume since its quantum yield in the immediate surroundings may be uncertain or is likely to be different from that in pure solvent. Moreover, the complex milieu of the cell can result in non-uniform distribution of fluorophore among different spatial locations in the cell. Often a more reliable way of measuring fluorescence intensity of an intracellular probe A is to normalize or ratio it with emission intensity of a reference probe B that is covalently linked with it (Figure 2)[52]. Ratio imaging served as a useful analytical tool for the cell interior[53–55] before fluorescence lifetime imaging (FLIM) techniques arrived.

Fluorescence lifetime

The fluorescence lifetime $\langle\tau\rangle$ (Figure 3) which bears a tell-tale sign of the probe, is defined as follows[50]

$$\langle\tau\rangle = 1/(k_r + k_{nr}), \quad (2)$$

where k_r and k_{nr} refer to rate constants of radiative and non-radiative processes that contribute to the decay of

excited fluorophore to ground state (S_0 in Figure 3) respectively.

Unlike fluorescence intensity this kinetic parameter is independent of fluorophore concentration in the dilute regime (nM–μM), making it a signature parameter to ascertain intracellular environment surrounding the probe. Decrease in τ indicates fluorescence quenching of donor arising from either a spatially distant acceptor probe by Förster resonance energy transfer (FRET), or a nearby collisional quencher. Mapping the fluorescence lifetime of the probe in the intracellular space by techniques like FLIM[56,57] can yield a wealth of information on protein–protein interactions, ligand binding and other events[58,59].

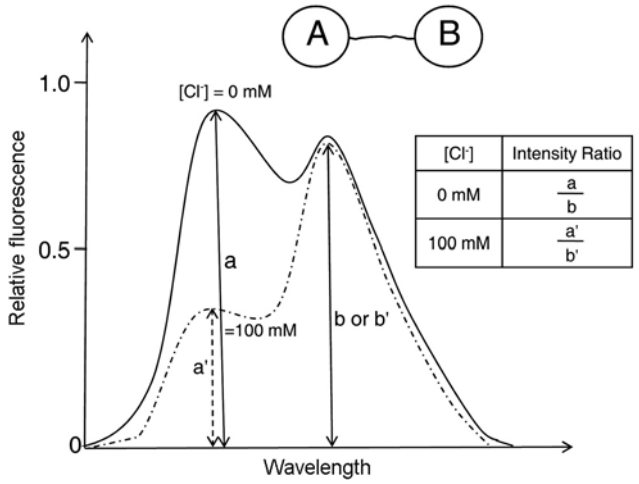

Figure 2. Fluorescence intensity ratio. The fluorescence emission spectrum of probe *A* is sensitive to chloride concentration in surrounding medium, while that of probe *B* is not. Intensity ratio from the covalently linked pair *A*–*B* can serve as an indicator of intracellular chloride ion concentration that is independent of the concentration of *A*–*B*.

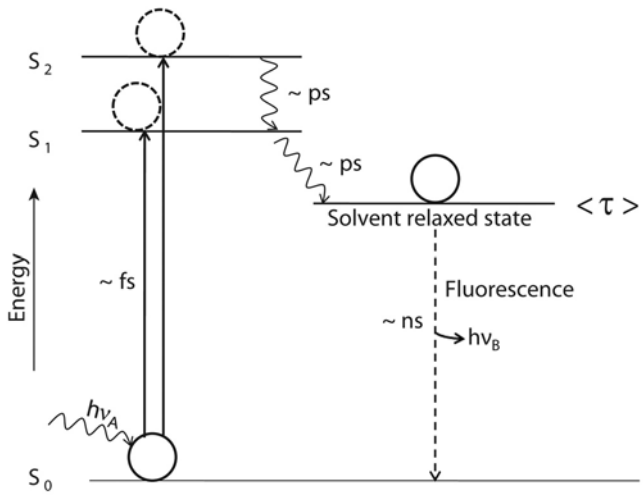

Figure 3. Fluorescence lifetime, i.e. the average time $\langle \tau \rangle$ spent by a fluorophore in the excited state (typically 0.1–10 ns).

Fluorescence anisotropy

The fluorescence anisotropy r of a probe can reveal information on the Brownian rotational motion of the probe[50]. The anisotropy r and time-dependent decay of anisotropy $r(t)$ are defined as follows

$$r = \frac{I_{\text{par}} - I_{\text{per}}}{I_{\text{par}} + 2I_{\text{per}}}, \tag{3}$$

$$r(t) = \frac{I_{\text{par}}(t) - I_{\text{per}}(t)}{I_{\text{par}}(t) + 2I_{\text{per}}(t)}, \tag{4}$$

$$r(t) = r_0 \left\{ \alpha \exp\left(-\frac{t}{\phi_{\text{fast}}} \right) + (1-\alpha) \exp\left(-\frac{t}{\phi_{\text{slow}}} \right) \right\}, \tag{5}$$

where I_{par} and I_{per} refer to fluorescence intensity at polarizations parallel and perpendicular to that of incident light respectively, while r_0 refers to initial anisotropy of the fluorophore and α denotes the fractional amplitude of fast rotational correlation time component ϕ_{fast} in the anisotropy decay.

Fluorescence anisotropy or polarization now enjoys wide popularity in clinical and high-throughput assays. It has been employed for ligand binding, immunoassays, high throughput screening and live cell imaging, as reviewed recently[60]. Polarization imaging, for example, enables us to spatially map the steady-state anisotropy of the probe at different regions of the cell as first demonstrated by Axelrod[61] to monitor orientation of carbocyanine in erythrocyte ghosts. Later, Gough and Taylor[62] used polarization imaging to investigate binding of fluorescein isothiocyanate (FITC)-calmodulin to different regions of serum-starved fibroblasts in response to stimulation with media containing serum.

The time-dependent decay in $r(t)$ at sub-nanosecond resolution can be measured using time-domain[63] or frequency-domain[64] techniques. Analysis of such anisotropy decays can reveal the rotational correlation time (ϕ) of the fluorophore in the intracellular milieu (Figure 4)[65–70]. For the specific case shown in Figure 4 *a*, $r(t)$ can be fitted according to eq. (5). The magnitude of ϕ is dependent on the micro-viscosity experienced by the probe inside the cell and the hydrodynamic volume of the free probe or probe-bound macromolecule.

Measuring diffusion of probes/proteins inside living cells using fluorescence microscopy

Diffusive or Brownian motion inside a cell arises from the thermal jiggling of water molecules. Diffusion is a form of passive transport in cells that is most effective (or fast) at distances < 100 μm. For example, while diffusion

can carry molecular oxygen to different regions of a small organism (1–50 μm), more complex mechanisms are necessary to circulate O_2 to all tissues in humans and larger animals.

The diffusion of a small tracer molecule like a fluorescent dye ($M_w \sim 500$ Da) or a medium-sized protein like GFP ($M_w \sim 30$ kDa) inside the complex spatial landscape of a living cell can depend on multiple factors like: (a) the physical structure of the tracer molecule and structure of the intracellular surroundings it is traversing around and (b) the interactions between the tracer and internal molecules of the cell. Measuring the translational diffusion coefficients of fluorescent probes inside cells using techniques like FRAP have revealed the extent to which molecular crowding in the cytoplasm or mitochondrial matrix can hinder diffusion of solutes and macromolecules. Diffusion of tracer molecules in membranes has shed light on its anomalous nature in such environments[71]. In this article we briefly highlight experimental approaches that enable measurement of diffusion inside cells and organelles.

Measurement of translational diffusion

Two commonly employed methods to measure translational diffusion of fluorescent molecules are FCS and FRAP that is also referred sometimes as fluorescence photobleaching recovery (FPR). For the interested reader, an elegant comparison between FCS and FRAP techniques has been carried out previously[72].

FCS operates in the single fluorescent molecule concentration regime where just a handful of fluorophores are interacting with their surroundings in an unbounded but optically confined volume of few femtolitres. The elegance of FCS stems from the fact that it is a perturbation-free technique to measure diffusion. Essentially the method exploits the tiny deviations from average fluorescence intensity (equilibrium) to measure diffusivity. The reader is directed to an excellent review on the theory and applications of FCS to observe intracellular diffusion[73]. Other than FCS and FRAP, single-particle tracking methods which employ time-dependent fluorescence images for tracking, have revealed trajectories of individual proteins or lipids on the plasma membrane of cells. Apart from Brownian motion, non-Brownian motion like directed motion and anomalous diffusion have also been observed in such trajectories[71].

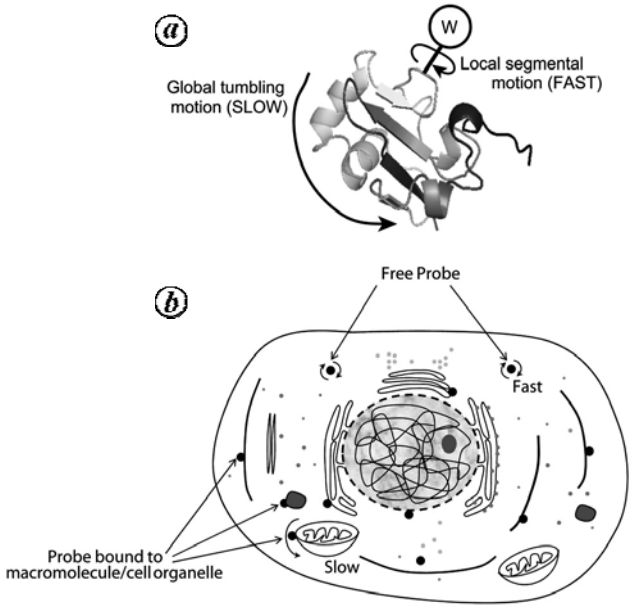

Figure 4. Fluorescent probe rotation. ***a***, The rotational correlation time of a fluorescent probe (like tryptophan) covalently linked to a macromolecule (like protein) can have two components. A fast component, ϕ_{fast} arising from localized rotational freedom in the vicinity of the attachment site and a slow component ϕ_{slow} from the overall rotation of the whole macromolecule. ***b***, A fluorescent probe inside a cell can be free in fluid phase or bind to a large or stationary organelle/macromolecule in the cellular milieu. The rotational motion of such a probe can reveal two components. A fast component, ϕ_{fast} arising from rotation of freely diffusing probe and a slow component, ϕ_{slow} arising from overall rotation of probe–macromolecule complex.

Fluorescence recovery after photobleaching

Unlike FCS, FRAP data are ensemble-averaged. In a sea of fluorophores restricted by a confined space (like the cell interior), FRAP is initiated by rapid and sudden creation of a depletion in fluorescence within a spatially defined spot (1–5 μm) by irreversible photobleaching. The recovery of fluorescence in the bleached spot arises from diffusion of nearby fluorophores that attempt to replenish the loss of fluorophores at the bleached spot (Figure 5). The rate of fluorescence recovery after photobleaching is chiefly determined by the diffusion coefficient of the fluorophore provided other determinant

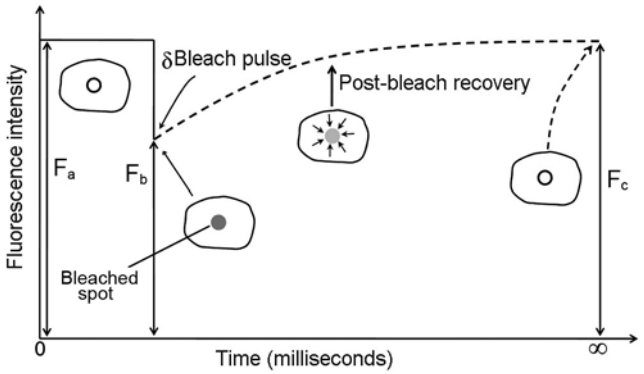

Figure 5. Fluorescence recovery after photobleaching. The typical variation in fluorescence intensity collected from a bleach spot with time during a spot photobleaching experiment is shown. A pictorial representation of the bleach zone at different times highlighting diffusion is also shown. See Figure 10 for comparison of bleach zone profile in TIR-FRAP and spot photobleaching.

instrumental parameters are held invariant. It is important that the following caveats are kept in mind:

1. The duration of photobleaching needs to be kept small (10–100 μs) in comparison to the recovery period (1–100 ms) to avoid complications arising from diffusion of fluorophores during photobleaching.
2. The fractional loss of fluorescence due to photobleaching (= $(F_a - F_b)/F_a$) must be kept within 25–45% of pre-bleach fluorescence (F_a) from the bleach spot. This is to ensure that depletion of fluorophore population owing to photobleaching is negligible in comparison to total fluorophore population in the confined space. Consequently, the recovery of fluorescence post-bleach shall eventually reach levels (F_c) nearly matching pre-bleach fluorescence.
3. The intensity of excitation light during the recovery phase must be well below intensities that can cause photobleaching of fluorophores contributing to recovery of fluorescence. If not, the recovery profile instead of displaying a monotonic rise can display a rise at early times followed by a decline at much later times ($t = \infty$), resulting in F_c that is significantly lower than F_a. In the absence of photobleaching during the recovery phase, the fluorescence collected at much later times is expected to show a flat horizontal profile with time.
4. Reversible photobleaching recovery arises when fluorophores in the bleach zone populate (or hide in) the long-lived triplet electronic state for a few milliseconds, followed by their decay to ground state and subsequent excitation during the recovery phase giving rise to fluorescence. This reversible photobleaching recovery has no contribution from diffusion, making it undesirable in FRAP measurements. One can suspect occurrence of reversible photobleaching if $t_{1/2}$ (see below) shows no change with change in size of the bleached spot (achieved by changing illumination objective magnification).

The half-time for recovery, $t_{1/2}$ in FRAP data can be obtained by numerically solving the eq. (6) below

$$F(t_{1/2}) = (F(\infty) - F(0))/2, \tag{6}$$

where $F(\infty) = F_c$ and $F(0) = F_b$ as shown in Figure 5. The percentage recovery is defined as

$$\% \text{ recovery} = \left\{ \frac{F_c - F_b}{F_a - F_b} \right\} \times 100. \tag{7}$$

The relative viscosity of cytoplasm compared to water can be determined by comparing $t_{1/2}$ observed for the probe in cytoplasm (from irreversible recovery process) with that measured for diffusion of the same probe in solutions of known viscosity (see later in the text).

In the absence of photobleaching during the recovery period, a decrease in F_c in comparison to F_a would imply the presence of an immobile fraction (= $(F_a - F_c)/F_a$). Such a fraction can arise when a significant number of fluorescent probes are bound to large macromolecules in the cell interior, thereby drastically slowing down their mobility.

FRAP was previously employed to observe the lateral diffusion of proteins in plasma membranes of animal cells[74]. However, it has been adopted to study all aspects of cell biology today[75–81].

The instrumental design employed to carry out most FRAP experiments described in this article is depicted in Figure 6. More in-depth details on the instrumentation are available elsewhere[82]. Briefly, the above apparatus was constructed to measure sub-millisecond fluorescence recovery processes in living cells. The intensity of a continuous-wave argon-ion laser was modulated to rapidly rise (< 1 μs) by 10^6 fold during the period of the bleach pulse (10–100 μs) using two acousto-optic modulators in series. The emitted fluorescence was detected by a photomultiplier tube (PMT) that was subsequently amplified and digitized at 1 MHz. The PMT was carefully protected from the intense flash during the bleach pulse by reducing its gain around ~1500-fold using a computer-controlled gating circuit.

The translational diffusion of the fluorescent probe 2′,7′-Bis-(2-carboxyethyl)-5-(and-6)-carboxyfluorescein (BCECF)[83] in the cytoplasm of 3T3 fibroblasts was measured by Kao and co-workers[84] in 1993 using FRAP technique. The diffusion coefficient of BCECF in the cytoplasm was observed to be 3.7-fold slower compared to water. It was identified that translational diffusion of the probe in the cytoplasm was hindered by increased fluid-phase viscosity, transient binding of probe to immobile cytoplasmic components and most importantly, frequent collisions of the probe with cell solids. In the above study, BCECF was introduced into the cytoplasm of 3T3 fibroblasts by incubating its acetoxymethyl ester derivative (BCECF-AM) that is membrane permeant with cells in PBS medium at 37°C. The BCECF-AM ester linkages are hydrolysed by non-specific intracellular esterases yielding the parent compound with four negative charges. This charged BCECF is retained in the cytoplasm for sufficient time to permit fluorescence measurements.

The advent of GFP as an endogenous non-invasive marker for gene expression and protein localization[36] permitted investigations on the diffusion of macromolecular-sized solutes inside living cells without resorting to traumatic procedures like microinjection. An added advantage was that GFP could be easily expressed as a fusion protein with known endogenous protein markers achieving targeted expression of GFP in specific organelles or subcellular sites.

The translational diffusion of GFP-S65T variant in the cytoplasm of Chinese Hamster ovary cells (CHO-K1)

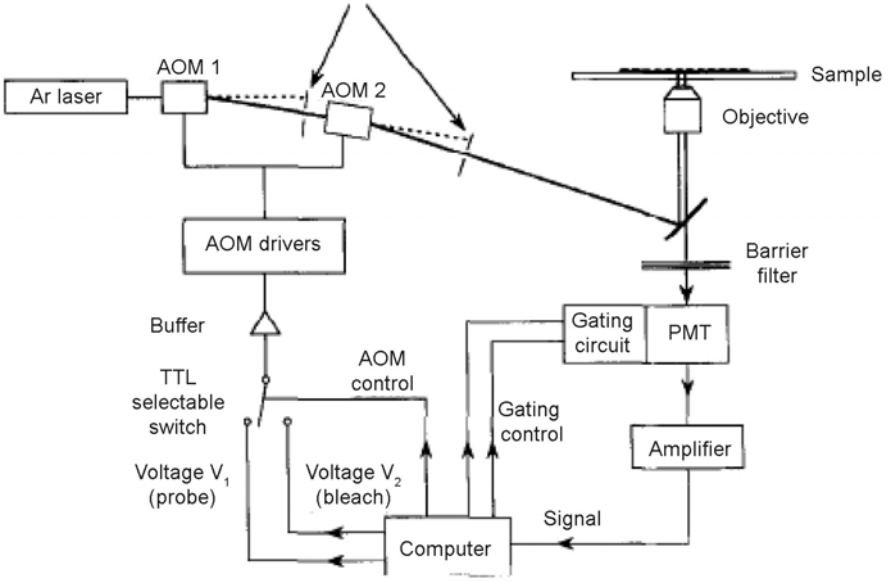

Figure 6. Schematic of the spot photobleaching recovery apparatus. The beam from a continuous-wave Ar laser was modulated by two acousto-optic modulators (AOM 1 and AOM 2) and directed onto the stage of a fluorescence microscope configured here for epi-illumination. The computer sets probe (V_1) and bleach (V_2) voltages to drive the AOMs, activates the photomultiplier protection circuit (gating circuit) and digitizes the amplified photomultiplier anode current. Reprinted with permission from ref. 82.

using FRAP was reported by Swaminathan and coworkers[85] in 1997. Figure 7 displays the GFP fluorescence recovery curves both from reversible photobleaching (Figure 7 *a*) and diffusion-mediated slow recovery (Figure 7 *c*) observed at different relative cell volumes using FRAP. The FRAP recovery was ~ 82% complete, suggesting that majority of GFP-S65T was mobile in cytoplasm. The $t_{1/2}$ for irreversible fluorescence recovery process was measured as ~ 83 ms in cytoplasm, yielding a relative viscosity of 3.2 in cytoplasm in comparison to water (Figure 7 *b*). Measurement of GFP diffusion with 19 and 70 kDa dextrans revealed that this relative viscosity is equivalent to a dextran concentration of ~ 8% w/w (Figure 7 *d*). Figure 7 *c* reveals that swollen cells show accelerated recovery, while shrunken cells display slow recovery in comparison to cells under isoosmotic conditions (relative cell volume = 1.0). These changes in recovery kinetics are accounted by dilution (contributing to faster recovery) or enhancement (slower recovery) of obstacle concentration in cell cytoplasm, which dictates GFP mobility in cytoplasm[84].

It was important to study how the densely crowded mitochondrial matrix, the site of tricarboxylic acid cycle and fatty acid oxidation pathway can obstruct the diffusion of GFP. Previous work has argued that diffusion of metabolites and small solutes in the aqueous phase may be severely hampered in the matrix owing to crowding. To verify this, diffusion of GFP expressed in mitochondrial matrix of fibroblast, liver, skeletal muscle and epithelial cell lines was observed using FRAP. Mathematical analysis of observed data using a model for diffusion of GFP in the matrix yielded GFP diffusion coefficients that were only 3–4-fold less than in water[86]. The rapid translational diffusion of GFP in the mitochondrial matrix implies that metabolite channelling may not be essential to surmount diffusive barriers.

Earlier work had shown that translational diffusion of microinjected FITC-dextrans (molecular weight, 4–2000 kDa) and FITC-Ficolls (R_G, 40–300 Å) in Swiss 3T3 fibroblast and Madin-Darby Canine Kidney epithelial cells (MDCK) cytoplasm was slowed down 3–4-fold in comparison to water[87]. Diffusion in the nucleus of the same cells for FITC-dextrans and FITC-Ficolls of the sizes mentioned above, was also slowed down ~4-fold. Importantly, the slowing down observed in cytoplasm and nucleus was independent of the size of the dextrans and Ficolls employed, arguing against the concept of solute sieving (size-dependent diffusion) in cytoplasm[88].

The epifluorescence microscopy techniques discussed above do not permit selective excitation or illumination of a chosen tiny spatial volume inside the cell sample. There are multiple approaches to achieve this spatial selectivity. Multiphoton fluorescence excitation is one of them. A simpler way to selectively illuminate a small spatial volume in the cell is to use total internal reflection fluorescence (TIRF) microscopy[89,90]. TIRF uses an evanescent wave for exciting fluorophores that has a limited penetration depth (~ 100 nm) in the cell interior beyond the cell membrane interface depending on the incident angle. As a consequence, only fluorophores in membrane-adjacent cytoplasm receive enough excitation energy to emit fluorescence, while fluorophores localized deeper in

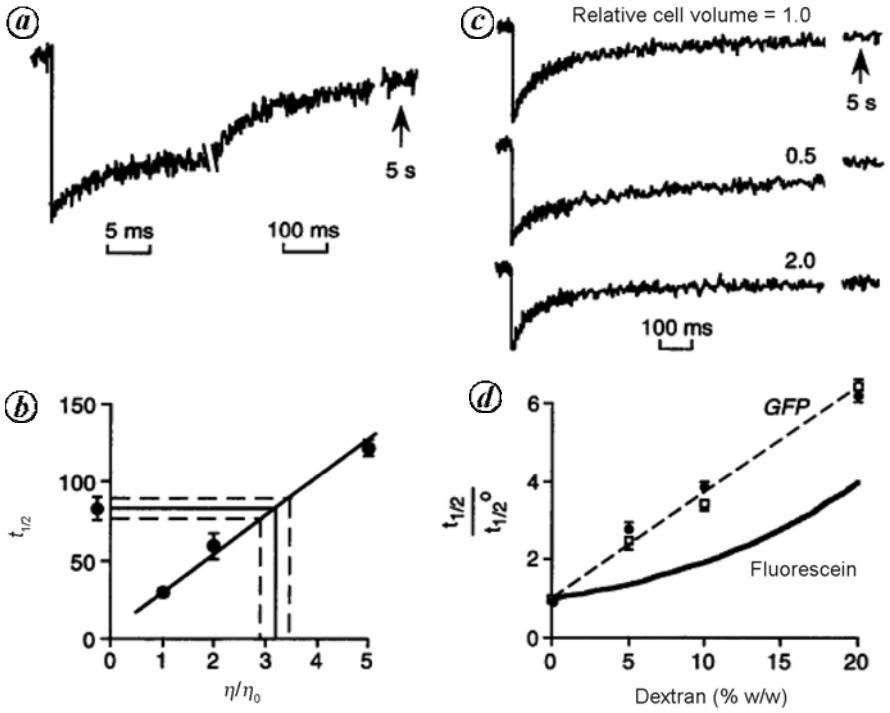

Figure 7. Translational diffusion of GFP-S65T in cytoplasm. ***a***, Spot photobleaching (20X objective) was carried out in cells expressing GFP-S65T using 50 μs bleach time. Note the presence of a fast recovery process from reversible photobleaching and slower recovery resulting from GFP diffusion. ***b***, Determination of relative cytoplasmic viscosity. Recovery half-times ($t_{1/2}$, in ms) for GFP-S65T diffusion in PBS containing glycerol plotted against relative solution viscosity. Data for GFP-S65T diffusion in cytoplasm are indicated. ***c***, Recovery curves as in (***a***) for cells in PBS (relative volume, 1.0) and after brief incubation with PBS containing 300 mM sucrose (relative volume, 0.5) or 1 : 1 PBS : water (relative volume 2.0). ***d***, Influence of solution crowding on GFP-S65T diffusion. Solutions consisted of GFP-S65T in PBS containing indicated concentrations of dextran (19 kDa, squares; 70 kDa, filled circles). The ordinate is $t_{1/2}$ for photobleaching recovery with versus without ($t^0_{1/2}$) dextran. The curve for diffusion of fluorescein was taken from Kao *et al.*[84] and confirmed. Reprinted with permission from ref. 85.

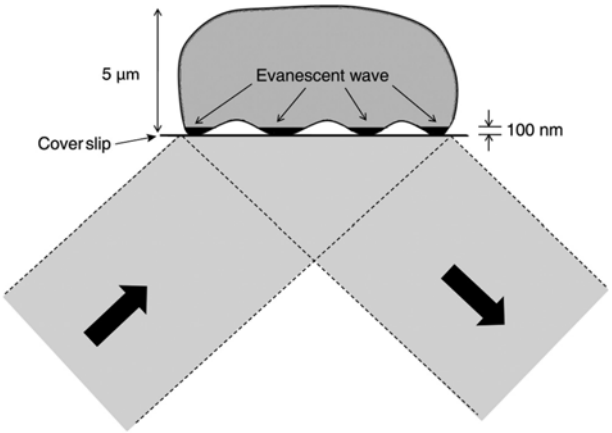

Figure 8. TIR excitation at membrane adjacent cytoplasm. TIR fluorescence image can reveal the distinct regions of focal contacts in the cell shown here. Selective excitation of fluorophores near the membrane interface is made possible by the exponential decay of the evanescent field in *z*-axis.

the cell interior far from the membrane remain unexcited and therefore dark (Figure 8). TIRF microscopy is therefore suited to investigate dynamic biological events in the cytoplasmic space very close to the membrane[91–93].

It was worthwhile to study if and how diffusion of a fluorescent probe in the membrane-adjacent cytoplasm is different from the bulk cytoplasm. The ideal way to observe such a diffusion was to measure fluorescence photobleaching recovery profile using an evanescent wave excitation from a TIRF set-up, hereafter referred to as TIR-FRAP. A schematic of the instrumental set-up for TIR-FRAP[94] is shown in Figure 9. It is pertinent to note that the evanescent wave excitation is generated using a quartz prism that is optically coupled to quartz coverslip containing growing cells (inverted) using glycerol to maintain continuity in refractive index. Additionally, the atmosphere around the cells was controlled and filled with oxygen to eliminate reversible photobleaching recovery which does not originate from diffusion and can interfere with irreversible photobleaching recovery analysis.

TIR-FRAP differs from conventional spot photobleaching carried out using an epifluorescence set-up (Figure 1) in several respects. First, the bleach zone geometry in TIR-FRAP differs significantly compared to spot photobleaching as shown in Figure 10. As a consequence of a shallow bleach depth (~ 100 nm), fluorescence recovery in TIR-FRAP is rapid and can be approximated to

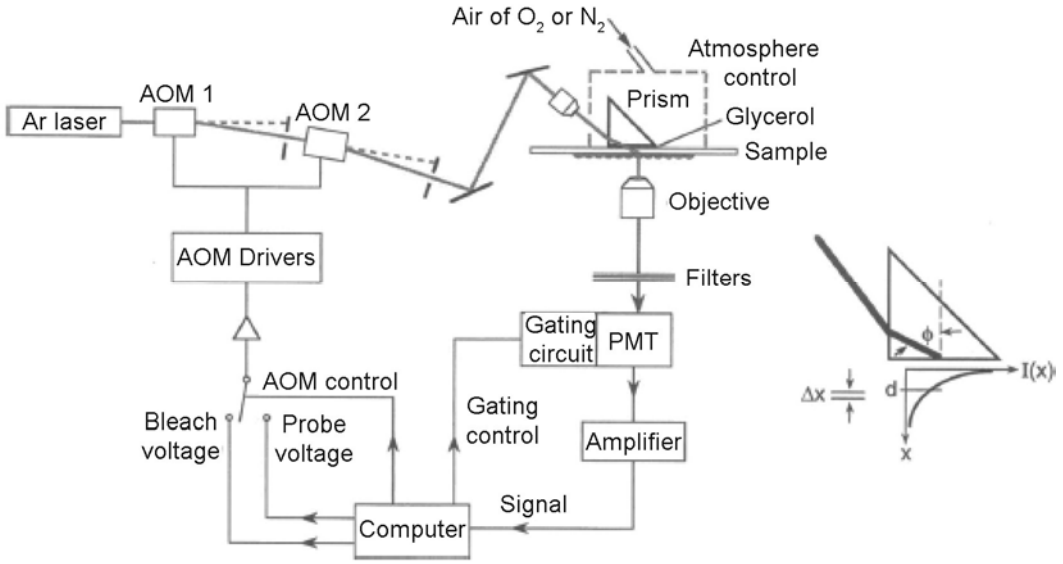

Figure 9. (Left) Schematic of TIR-FRAP instrumentation. The beam from an Ar ion laser was modulated by serial acousto-optic modulators and directed onto the sample through a 25X objective lens and right triangular fused silica prism. The signal was filtered and detected by a gated photomultiplier. (Right) Expanded view of prism showing beam incident angle, ϕ and evanescent field depth, d. Reprinted with permission from ref. 94.

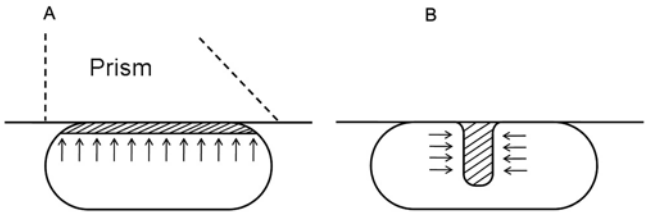

Figure 10. Bleach spot geometry. A, Shallow depth of TIR-FRAP bleach spot near the membrane owing to decaying evanescent field. The arrows highlight diffusion of unbleached fluorophores to the bleached zone. B, Deep cylindrical well of bleached fluorophores created by spot photobleaching. Fluorescence recovery at the bleached spot by two-dimensional diffusion of unbleached fluorophores is indicated by arrows.

essentially one-dimensional diffusion of unbleached fluorophores in contrast to spot photobleaching, where recovery of fluorescence occurs by two-dimensional diffusion. Secondly, the fast kinetics of fluorescence recovery in TIR-FRAP can experience competition from reversible photobleaching recovery.

The translational diffusion of BCECF in the membrane adjacent cytoplasm of MDCK cells using TIR-FRAP was first reported by Swaminathan and co-workers[94] in 1996. In this work a mathematical model was developed to calculate the diffusion coefficient of bleached fluorescent probe from bleach parameters, time-course of TIR-FRAP recovery (including both reversible and irreversible components) and evanescent field depth. TIR-FRAP measurements were carried out with fluorescein in aqueous solutions to validate the model. Diffusion coefficients of FITC-dextrans in the molecular mass range (10–2000 kDa) were compared using both spot photobleaching and TIR-FRAP techniques to reveal nearly matching values. The reversible photobleaching observed for intracellular BCECF in TIR-FRAP measurements was effectively eliminated by saturating the medium with 100% oxygen that quenches the triplet state population. In the absence of reversible photobleaching, diffusion of BCECF in MDCK cytoplasm bathed in oxygen-saturated solution (Figure 11 *a*) under the evanescent field revealed fast recovery curves (average $t_{1/2} \sim 4.5$ ms), with similar recovery kinetics for bleach times of 0.2, 0.6 and 1 ms (Figure 11 *a*). The diffusion of fluorescein in water measured under similar conditions (Figure 11 *c*) showed a $t_{1/2} \sim 0.4$ ms. Figure 11 *b* displays recovery under trans-illumination (where the prism is removed) covering several cells together, that shows no signs of reversible photobleaching recovery, owing to efficient quenching of the triplet state by oxygen. The calculations yielded a diffusion coefficient for BCECF in the membrane adjacent cytoplasm that was 6–10-fold greater than that in water. This implied a significant slowing of BCECF diffusion in the membrane adjacent cytoplasm compared to bulk cytoplasm.

Today photobleaching techniques have been replaced or complemented by photoactivation or photoconversion experiments that employ photomodulatable fluorescent proteins. These approaches require faster and less intense light exposure compared to photobleaching while allowing for tracking of fast protein movements with diffusion coefficients as large as 10^{-6} cm^2/s (ref. 77). Efforts are also underway for a more quantitative analysis of FRAP recovery curves to extract information related to binding interactions in the cell[75]. These are relevant to understand molecular networks.

Measurement of rotational diffusion

The random Brownian rotational motion (tumbling) of a small fluorescent dye like BCECF or a large protein like GFP is another indicator of the local micro-viscosity surrounding the probe. The rotational correlation time of BCECF in PBS is ~ 0.25 ns at room temperature (24°C)[95], while the same for a macromolecule like GFP (~ 30 kDa) is 20 ns (ref. 85). Contrast this timescale with $t_{1/2}$ times around ~ 30 ms observed during GFP FRAP recovery for bleach spot size of 5 μm diameter[85]. This reveals the variation in disruption of solvent structure (like in hydrogen-bonded water) during translational and rotational diffusion that is driven by the same thermal forces.

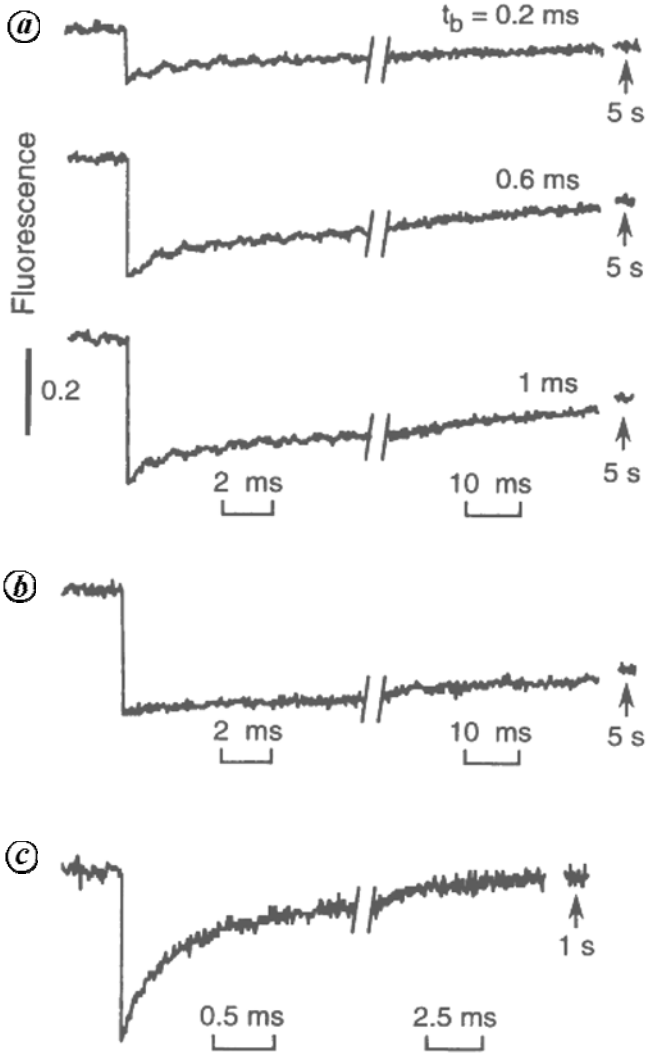

Figure 11. Translational diffusion of BCECF in MDCK cytosol measured by TIR-FRAP. ***a***, TIR-FRAP measurements with indicated bleach times. ***b***, Measurement identical to that in ***a*** (1 ms bleach time) with prism removed (for transillumination). ***c***, TIR-FRAP measurement of diffusion of fluorescein (1 mM) in PBS with 0.1 ms bleach time. The averaged fluorescence at the indicated late time (after which essentially all recovery has occurred) is shown. Reprinted with permission from ref. 94.

The construction of a frequency-domain epifluorescence microscope for measuring fluorescence intensity and anisotropy decays of fluorophores in subcellular domains has been reported previously by Verkman and co-workers[96]. The authors list a number of conditions that must be satisfied to enable microscopy measurements of multi-component fluorescence intensity decays in living cells like: (1) Measurements must be rapid (< 60 s) with high detection efficiency to minimize phototoxicity. (2) Reference solutions for lifetime data acquisitions must be introduced without altering the cell position or objective focus. (3) There must be no depolarization of excitation or emission light by microscope components like dichroic mirror and objective. (4) Subtracting background fluorescence like autofluorescence from sample signal must be convenient. (5) Time resolution in data must be adequate to capture fast (0.1–5 ns) and slow (10–100 ns) rotational motions. (6) Spatial resolution must be below 5% of cell dimensions. To meet criterion (1) frequency-domain based approaches are more suited compared to time-domain techniques.

The viscosity in the aqueous domain of 3T3 fibroblasts was measured by phase modulation microfluorimetry[95]. Fushimi and Verkman measured the picosecond rotational correlation time of three fluorescent probes, namely BCECF, 6-carboxyfluorescein and 8-hydroxypyrene-1,3,6-trisulphonic acid (HPTS) inside the cytoplasm of 3T3 fibroblasts. As highlighted in Figure 4 *b*, a fraction of the probe population can tumble freely in the aqueous phase of the cytoplasm contributing to the fast component of anisotropy decay, while the remaining fraction can remain non-covalently bound to a macromolecule in the cytoplasm slowing down its rotational correlation time. The component α in eq. (5) represents the free fraction of the probe. In the work above it was observed that while BCECF had a ϕ_{fast} of ~ 294 ps, the remaining two dyes showed a value ~ 180 ps. The value of α was ~ 0.78 for BCECF, while it was ~ 0.6 for the other two dyes. These results yielded a relative fluid-phase cytoplasmic viscosity (η/η_0) in the region of 1.2–1.4 compared to water in Swiss 3T3 fibroblasts. Later work by Bicknese and co-workers[97] from the same lab revealed that fluid-phase cytoplasmic viscosity in the membrane adjacent cytoplasm of Swiss 3T3 fibroblasts and MDCK cells was in the region of (1.0–1.1) ± 0.2 cP, not significantly different from the values observed for bulk cytoplasm far from the plasma membrane.

The rotational diffusion of GFP-S65T in PBS solutions[85] revealed a ϕ_{fast} of 0.74 ns and ϕ_{slow} of 19 ns with component α near 0.09, according to Figure 4 *a* and eq. (5). This suggests limited freedom for mobility of the chromophore in the interior of GFP causing major loss in anisotropy by slow global motion of the entire GFP molecule. Inside the cytoplasm of CHO-K1 cells (Figure 12)[85], GFP revealed a fluorescence lifetime of 2.6 ns (Figure 12 *a*, compared to 2.9 ns in PBS) and rotational

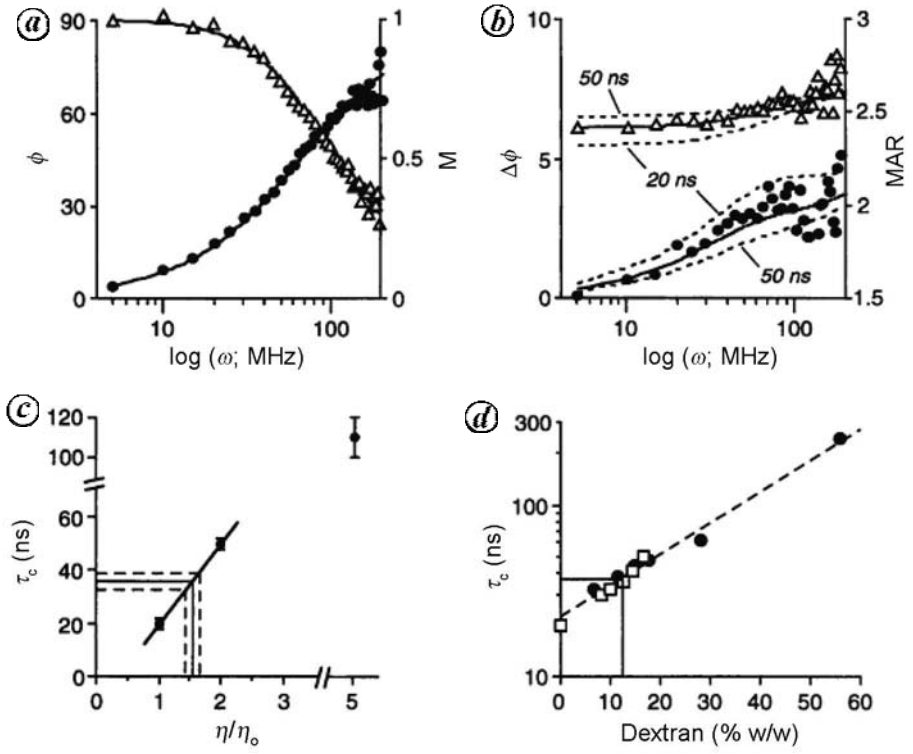

Figure 12. Rotational diffusion of GFP-S65T in cytoplasm. ***a***, Phase-modulation plot of GFP-S65T lifetime in cytoplasm. The fitted lifetime was 2.6 ns. ***b***, Differential phase-modulation plot of GFP-S65T anisotropy decay with correlation times of 34 ns (fractional amplitude, 0.85) and 0.3 ns. Dashed curves indicate where the data would fall for correlation times of 20 and 50 ns instead of 34 ns. ***c***, Determination of relative cytoplasmic viscosity. Rotational correlation times for GFP-S65T in PBS containing glycerol plotted against relative solution viscosity. Data for GFP-S65T rotation in cytoplasm are indicated. ***d***, Dependence of GFP-S65T rotational correlation time on dextran concentration for 19 kDa (squares) and 70 kDa (filled circles) dextrans. Reprinted with permission from ref. 85.

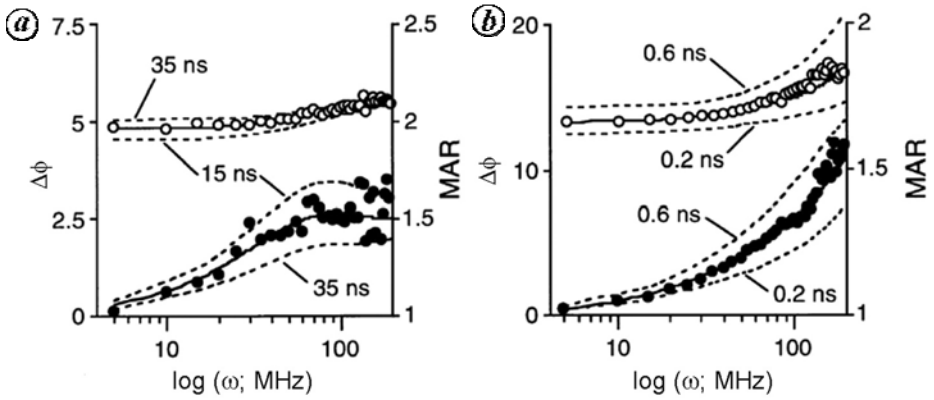

Figure 13. Rotation of BCECF and GFP in the mitochondrial matrix measured by time-resolved anisotropy. Phase-modulation plots of differential phase angle (filled circles) and modulation factor (open circles) as a function of modulation frequency. ***a***, GFP rotation in the mitochondrial matrix of CHO cells. Fitted curves correspond to a rotational correlation time of 21.4 ns (lifetime 2.5 ns, limiting anisotropy $r_0 = 0.4$). Dashed curves shown for 15 and 35 ns correlation times. ***b***, Rotation of BCECF in the matrix of isolated liver mitochondria. Curves correspond to rotational correlation times of 0.35 and 46 ns with a fractional amplitude of the fast component of 0.56 (lifetime 3.6 ns, $r_0 = 0.392$). Dashed curves shown for short correlation times of 0.2 and 0.6 ns. Reprinted from ref. 86.

correlation times of 0.3 (ϕ_{fast}) and 34 ns (ϕ_{slow}), with component α near 0.15 (eq. (5); Figure 12 *b*). The slowing down in global rotational motion of GFP in the cellular milieu was comparable to a similar effect observed with GFP in the presence of: (a) 12% w/w dextrans (19 or 70 kDa) in PBS (Figure 12 *d*) and (b) 1.5-fold viscous saline in PBS–glycerol mixture (Figure 12 *c*). The slightly slower rotation of GFP in the cytoplasm compared to

BCECF was attributed to steric interactions with intracellular macromolecules.

The rotational motion of BCECF and GFP in the crowded mitochondrial matrix can shed light on the restrictions or the lack of it on the mobility of these differently sized fluorescent probes. The rotational diffusion of BCECF inside freshly isolated mitochondria from rat liver was examined (Figure 13 *b*)[86]. Analysis of BCECF anisotropy decay inside isolated mitochondria revealed a ϕ_{fast} of 0.32 ns ($\alpha = 0.51$) arising from free BCECF rotation and ϕ_{slow} of 59 ns from bound BCECF. The rotational correlation time for tumbling of whole GFP in the mitochondrial matrix (Figure 13 *a*) was observed to be 23 ns (ref. 86), close to a value of ~20 ns observed in water[85]. No evidence for bound GFP in the matrix was observed. The free and rapid diffusion of BCECF and GFP in the mitochondrial matrix suggested that metabolite channelling for movement of metabolites may not be essential.

It is worthwhile to note that viscosity sensed by fluorescent probe under rotational diffusion is significantly less than that sensed under translational diffusion. This observation is in agreement with the notion that probe rotation is comparatively unhindered when probe size is smaller than spacings between obstacles[98]. Thus the probe is more likely to encounter collisions with obstacles in its path during translational diffusion than during rotational diffusion.

Today techniques like FLIM provide an option to record time-resolved fluorescence anisotropy images[66], but the complexity of the technique and the accompanying data analysis have made these applications rare. Instead of measuring parallel and perpendicularly polarized components of the time-resolved fluorescence over a whole image, selecting a region of interest or a single 'spot' and recording anisotropy decays appears an improved approach. The latter delivers better statistics in the anisotropy decays with typically shorter acquisition times, but at the cost of losing spatial variations in the anisotropy.

Cross-linking among labelled IgE receptors and their role in nanoscale membrane order were investigated by time-resolved anisotropy measurements on little-defined regions of interest[99]. It was stated that the cross-linking produced ordered domains that act to facilitate signalling. Polarization-difference imaging and time-resolved anisotropy have been recently used to study cancerous tissues. It was observed that Cybesin-stained cancerous tissue exhibited a higher anisotropy value than normal tissue[100], highlighting such contrast as a diagnostic tool for distinguishing cancerous and healthy tissues in clinical screening. Applications of fluorescence lifetime and polarization-resolved imaging in cell biology have been reviewed recently[59].

Perspective

The above results validate that fluorescence microscopy provides an important approach to monitor events like diffusion inside living cells. However, several challenges remain before one can use this technique to detect abnormal events *in vivo*. The major challenge is the lack of endogenous fluorescent probe that can act as a reporter for sensing abnormal biochemical changes inside the cell with the onset of disease and set alarm bells ringing.

1. Abbe, E., Beiträge zur Theorie des Mikroskops und der mikroskopischen Wahrnehmung. *Arch. Mikroskopische Anat*., 1873, **9**, 413–468.
2. Zheludev, N. I., What diffraction limit? *Nature Mater*., 2008, **7**, 420–422.
3. Klar, T. A., Engel, E. and Hell, S. W., Breaking Abbe's diffraction resolution limit in fluorescence microscopy with stimulated emission depletion beams of various shapes. *Phys. Rev. E*, 2001, **64**, 066613.
4. Thompson, M. A., Lew, M. D. and Moerner, W. E., Extending microscopic resolution with single-molecule imaging and active control. *Annu. Rev. Biophys*., 2012, **41**, 321–342.
5. Patterson, G., Davidson, M., Manley, S. and Lippincott-Schwartz, J., Super resolution imaging using single-molecule localization. *Annu. Rev. Phys. Chem*., 2010, **61**, 345–367.
6. Williams, D. B. and Carter, C. B., *Transmission Electron Microscopy: A Textbook for Materials Science*, Part 1, Springer Science + Business Media, New York, USA, 2009, pp. 3–22.
7. Koster, A. J. and Klumperman, J., Electron microscopy in cell biology: integrating structure and function. *Nature Rev. Mol. Cell Biol*., 2003, **4**, SS6–SS10.
8. Glaeser, R. M. and Taylor, K. A., Radiation damage relative to transmission electron microscopy of biological specimens at low temperature: a review. *J. Microsc*., 1978, **112**, 127–138.
9. McIntosh, J. R., Electron microscopy of cells: A new beginning for a new century. *J. Cell Biol*., 2001, **153**, F25–F32.
10. Stephens, D. J. and Allan, V. J., Light microscopy techniques for live cell imaging. *Science*, 2003, **300**, 82–86.
11. Masters, B. R., The development of fluorescence microscopy. In *Encyclopedia of Life Sciences*, John Wiley, Chichester, 2010, pp. 1–9.
12. Litchman, J. W. and Conchello, J. A., Fluorescence microscopy. *Nature Methods*, 2005, **2**, 910–919.
13. Spring, K. R., Fluorescence microscopy. In *Encyclopedia of Optical Engineering*, Marcel Dekker Inc, New York, USA, 2003, pp. 548–555.
14. Rao, J., Dragulescu-Andrasi, A. and Yao, H., Fluorescence imaging *in vivo*: recent advances. *Curr. Opin. Biotechnol*., 2007, **18**, 17–25.
15. Galdeen, S. A. and North, A. J., Live cell fluorescence microscopy techniques. *Methods Mol. Biol*., 2011, **769**, 205–222.
16. Ghiran, I. C., Introduction to fluorescence microscopy. In *Light Microscopy, Methods in Molecular Biology 689* (eds Garcia, H. C. and Melo, R. C. N.), Springer Science + Business Media, New York, USA, 2011, pp. 93–136.
17. Zhang, J., Campbell, R. E., Ting, A. Y. and Tsien, R. Y., Creating new fluorescent probes for cell biology. *Nature Rev. Mol. Cell Biol*., 2002, **3**, 906–918.
18. Wang, Y., Shyy, J. Y. J. and Chien, S., Fluorescence proteins, live-cell imaging, and mechanobiology: seeing is believing. *Annu. Rev. Biomed. Eng*., 2008, **10**, 1–38.
19. Wu, B., Piatkevich, K. D., Lionnet, T., Singer, R. H. and Verkhusha, V. V., Modern fluorescent proteins and imaging technologies to study gene expression, nuclear localization, and dynamics. *Curr. Opin. Cell Biol*., 2011, **23**, 310–317.
20. Shaner, N. C., Steinbach, P. A. and Tsien, R. Y., A guide to choosing fluorescent proteins. *Nature Methods*, 2005, **2**, 905–909.

21. Suárez, M. F. and Ting, A. Y., Fluorescent probes for super-resolution imaging in living cells. *Nature Rev. Mol. Cell Biol*., 2008, **9**, 929–943.
22. Giepmans, B. N. G., Adams, S. R., Ellisman, M. H. and Tsien, R. Y., The fluorescent toolbox for assessing protein location and function. *Science*, 2006, **312**, 217–224.
23. Day, R. N. and Davidson, M. W., The fluorescent protein palette: tools for cellular imaging. *Chem. Soc. Rev*., 2009, **38**, 2887–2921.
24. Yuan, L., Lin, W., Zheng, K., He, L. and Huang, W., Far-red to near infrared analyte-responsive fluorescent probes based on organic fluorophore platforms for fluorescence imaging. *Chem. Soc. Rev*., 2013, **42**, 622–661.
25. Wiedenmann, J., Oswald, F. and Nienhaus, G. U., Fluorescent proteins for live cell imaging: opportunities, limitations, and challenges. *IUBMB Life*, 2009, **61**, 1029–1042.
26. Alivisatos, A. P., Gu, W. and Larabell, C., Quantum dots as cellular probes. *Annu. Rev. Biomed. Eng*., 2005, **7**, 55–76.
27. Gao, X., Yang, L., Petros, J. A., Marshall, F. F., Simons, J. W. and Nie, S., *In vivo* molecular and cellular imaging with quantum dots. *Curr. Opin. Biotechnol*., 2005, **16**, 63–72.
28. Michalet, X. *et al.*, Quantum dots for live cells, *in vivo* imaging, and diagnostics. *Science*, 2005, **307**, 538–544.
29. Genger, U. R., Grabolle, M., Jaricot, S. C., Nitschke, R. and Nann, T., Quantum dots versus organic dyes as fluorescent labels. *Nature Methods*, 2008, **5**, 763–775.
30. Michalet, X., Siegmund, O. H. W., Vallerga, J. V., Jelinsky, P., Millaud, J. E. and Weiss, S., Detectors for single-molecule fluorescence imaging and spectroscopy. *J. Mod. Opt*., 2007, **54**, 239–281.
31. Michalet, X. *et al*., Development of new photon-counting detectors for single-molecule fluorescence microscopy. *Philos. Trans. R. Soc. B*, 2013, **368**, 20120035.
32. Joo, C., Balci, H., Ishitsuka, Y., Buranachai, C. and Ha, T., Advances in single-molecule fluorescence methods for molecular biology. *Annu. Rev. Biochem*., 2008, **77**, 51–76.
33. Sako, Y. and Yanagida, T., Single-molecule visualization in cell biology. *Nature Rev. Mol. Cell Biol*., 2003, **4**, SS1–SS5.
34. Walter, N. G., Single molecule detection, analysis, and manipulation. In *Encyclopedia of Analytical Chemistry* (ed. Meyers, R. A.), John Wiley, New Jersey, USA, 2008, pp. 1–10.
35. Gerdes, H. H. and Kaether, C., Green fluorescent protein: applications in cell biology. *FEBS Lett*., 1996, **389**, 44–47.
36. Tsien, R. Y., The green fluorescent protein. *Annu. Rev. Biochem*., 1998, **67**, 509–544.
37. Zimmer, M., Green fluorescent protein (GFP): applications, structure, and related photophysical behavior. *Chem. Rev*., 2002, **102**, 759–781.
38. Misteli, T. and Spector, D. L., Applications of the green fluorescent protein in cell biology and biotechnology. *Nature Biotechnol*., 1997, **15**, 961–964.
39. Matz, M. V., Lukyanov, K. A. and Lukyanov, S. A., Family of the green fluorescent protein: Journey to the end of the rainbow. *BioEssays*., 2002, **24**, 953–959.
40. Rubart, M., Two-photon microscopy of cells and tissue. *Circ. Res*., 2004, **95**, 1154–1166.
41. Centonze, V. E. and White, J. G., Multiphoton excitation provides optical sections from deeper within scattering specimens than confocal imaging. *Biophys. J*., 1998, **75**, 2015–2024.
42. So, P. T. C., Two-photon fluorescence light microscopy. In *Encyclopedia of Life Sciences*, Macmillan Publishers Ltd, Nature Publishing Group, New York, USA, 2002, pp. 1–5.
43. So, P. T. C., Dong, C. Y., Masters, B. R. and Berland, K. M., Two-photon excitation fluorescence microscopy. *Annu. Rev. Biomed. Eng*., 2000, **2**, 399–429.
44. McNeil, P. L., Direct introduction of molecules into cells. *Curr. Protocols Cell Biol*., 2003, 20.1.1–20.1.7.
45. Mobbs, P., Becker, D., Williamson, R., Bate, M. and Warner, A., Techniques for dye injection and cell labelling. In *The Plymouth Workshop Handbook* (ed. Ogden, D.), The Company of Biologists Ltd, Cambridge, UK, 1994, pp. 361–388.
46. Bao, G., Rhee, W. J. and Tsourkas, A., Fluorescent probes for live-cell RNA detection. *Annu. Rev. Biomed. Eng*., 2009, **11**, 25–47.
47. Andersson, H., Baechi, T., Hoechl, M. and Richter, C., Autofluorescence of living cells. *J. Microsc*., 1998, **191**, 1–7.
48. Hirstch, R. E., Hemoglobin fluorescence. In *Methods in Molecular Medicine, Hemoglobin Disorders: Molecular Methods and Protocols* (ed. Nagel, R. L.), Humana Press, Totowa, New Jersey, 2003, vol. 82, pp. 133–154.
49. Berezin, M. Y. and Achilefu, S., Fluorescence lifetime measurements and biological imaging. *Chem. Rev*., 2010, **110**, 2641–2684.
50. Lakowicz, J. R., *Principles of Fluorescence Spectroscopy*, Springer, Singapore, 2006, 3rd edn.
51. Johnson, I. D., Practical considerations in the selection and application of fluorescent probes. In *Handbook of Biological Confocal Microscopy* (ed. Pawley, J. B.), Springer Science + Business Media, New York, USA, 2006, pp. 353–367.
52. Jayaraman, S., Biwersi, J. and Verkman, A. S., Synthesis and characterization of dual-wavelength Cl^- sensitive fluorescent indicators for ratio imaging. *Am. J. Physiol*., 1999, **276**, C747–C757.
53. Bright, G. R., Fisher, G. W., Rogowska, J. and Taylor, D. L., Fluorescence ratio imaging microscopy. *Methods Cell Biol*., 1989, **30**, 157–192.
54. Dix, J. A. and Verkman, A. S., Mapping of fluorescence anisotropy in living cells by ratio imaging: application to cytoplasmic viscosity. *Biophys. J*., 1990, **57**, 231–240.
55. Tsien, R. Y. and Poenie, M., Fluorescence ratio imaging: a new window into intracellular ionic signalling. *Trends Biochem. Sci*., 1986, **11**, 450–455.
56. Becker, W., Fluorescence lifetime imaging – techniques and applications. *J. Microsc*., 2012, **247**, 119–136.
57. Periasamy, A. and Clegg, R. M. (eds), *FLIM Microscopy in Biology and Medicine*, CRC Press, Boca Raton, USA, 2010.
58. Sun, Y., Hays, N. M., Periasamy, A., Davidson, M. W. and Day, R. N., Monitoring protein interactions in living cells with fluorescence lifetime imaging microscopy. *Methods Enzymol*., 2012, **504**, 371–391.
59. Levitt, J. A., Matthews, D. R., Ameer-Beg, S. M. and Suhling, K., Fluorescence lifetime and polarization-resolved imaging in cell biology. *Curr. Opin. Biotechnol*., 2009, **20**, 28–36.
60. Jameson, D. M. and Ross, J. A., Fluorescence polarization/anisotropy in diagnostics and imaging. *Chem. Rev*., 2010, **110**, 2685–2708.
61. Axelrod, D., Carbocyanine dye orientation in red cell membrane studied by microscopic fluorescence polarization. *Biophys. J*., 1979, **26**, 557–573.
62. Gough, A. H. and Taylor, D. L., Fluorescence anisotropy imaging microscopy maps calmodulin binding during cellular contraction and locomotion. *J. Cell. Biol*., 1993, **121**, 1095–1107.
63. Steiner, R. F., Fluorescence anisotropy: theory and application. In *Topics of Fluorescence Spectroscopy* (ed. Lakowicz, J. R.), Plenum Press, New York, 1991, vol. 2, pp. 1–52.
64. Lakowicz, J. R., Cherek, H., Kuśba, J., Gryczynski, I. and Johnson, M. L., Review of fluorescence anisotropy decay analysis by frequency-domain fluorescence spectroscopy. *J. Fluoresc*., 1993, **3**, 103–116.
65. Gradinaru, C. C., Marushchak, D. O., Samim, M. and Krull, U. J., Fluorescence anisotropy: from single molecules to live cells. *Analyst*, 2010, **135**, 452–459.
66. Vogel, S. S., Thaler, C., Blank, P. S. and Koushik, S. V., Time-resolved fluorescence anisotropy. In *FLIM Microscopy in Biology*

and Medicine (eds Periasamy, A. and Clegg, R. M.), CRC Group, London, 2009, pp. 245–288.
67. Kawski, A., Fluorescence anisotropy: theory and applications of rotational depolarization. *Crit. Rev. Anal. Chem.*, 1993, **23**, 459–529.
68. LiCata, V. J. and Wowor, A. J., Applications of fluorescence anisotropy to the study of protein – DNA interactions. *Methods Cell Biol.*, 2008, **84**, 243–262.
69. Jameson, D. M. and Sawyer, W. H., Fluorescence anisotropy applied to biomolecular interactions. *Methods Enzymol.*, 1995, **246**, 283–300.
70. Owicki, J. C., Fluorescence polarisation and anisotropy in high throughput screening: perspectives and primer. *J. Biomol. Screen.*, 2000, **5**, 297–306.
71. Saxton, M. J. and Jacobson, K., Single-particle tracking: Applications to membrane dynamics. *Annu. Rev. Biophys. Biomol. Struct.*, 1997, **26**, 373–399.
72. Elson, E. L., Fluorescence correlation spectroscopy and photobleaching recovery. *Annu. Rev. Phys. Chem.*, 1985, **36**, 379–406.
73. Haustein, E. and Schwille, P., Fluorescence correlation spectroscopy: novel variations of an established technique. *Annu. Rev. Biophys. Biomol. Struct.*, 2007, **36**, 151–169.
74. Jacobson, K., Ishihara, A. and Inman, R., Lateral diffusion of proteins in membranes. *Annu. Rev. Physiol.*, 1987, **49**, 163–175.
75. Sprague, B. L. and McNally, J. G., FRAP analysis of binding: proper and fitting. *Trends Cell Biol.*, 2005, **15**, 84–91.
76. Reits, E. A. J. and Neefjes, J. J., From fixed to FRAP: measuring protein mobility and activity in living cells. *Nature Cell Biol.*, 2001, **3**, E145–E147.
77. Miyawaki, A., Proteins on the move: insights gained from fluorescent protein technologies. *Nature Rev. Mol. Cell Biol.*, 2011, **12**, 656–668.
78. Rayan, G., Guet, J. E., Taulier, N., Pincet, F. and Urbach, W., Recent applications of fluorescence recovery after photobleaching (FRAP) to membrane bio-macromolecules. *Sensors*, 2010, **10**, 5927–5948.
79. Schwartz, J. L., Snapp, E. and Kenworthy, A., Studying protein dynamics in living cells. *Nature Rev. Mol. Cell Biol.*, 2001, **2**, 444–456.
80. Carisey, A., Stroud, M., Tsang, R. and Ballestrem, C., Fluorescence recovery after photobleaching. *Methods Mol. Biol.*, 2011, **769**, 387–402.
81. Ankerhold, H. C. I., Ankerhold, R. and Drummen, G. P. C., Advanced fluorescence microscopy techniques – FRAP, FLIP, FLAP, FRET and FLIM. *Molecules*, 2012, **17**, 4047–4132.
82. Kao, H. P. and Verkman, A. S., Construction and performance of a photobleaching recovery apparatus with microsecond time resolution. *Biophys. Chem.*, 1996, **59**, 203–210.
83. Rink, T. J., Tsien, R. Y. and Pozzan, T., Cytoplasmic pH and free Mg^{2+} in lymphocytes. *J. Cell Biol.*, 1982, **95**, 189–196.
84. Kao, H. P., Abney, J. R. and Verkman, A. S., Determinants of the translational mobility of a small solute in cell cytoplasm. *J. Cell Biol.*, 1993, **120**, 175–184.
85. Swaminathan, R., Hoang, C. P. and Verkman, A. S., Photobleaching recovery and anisotropy decay of green fluorescent protein GFP-S65T in solution and cells: cytoplasmic viscosity probed by green fluorescent protein translational and rotational diffusion. *Biophys. J.*, 1997, **72**, 1900–1907.
86. Partikian, A., Ölveczky, B., Swaminathan, R., Li, Y. and Verkman, A. S., Rapid diffusion of green fluorescent protein in the mitochondrial matrix. *J. Cell Biol.*, 1998, **140**, 821–829.
87. Seksek, O., Biwersi, J. and Verkman, A. S., Translational diffusion of macromolecule-sized solutes in cytoplasm and nucleus. *J. Cell Biol.*, 1997, **138**, 131–142.
88. Luby-Phelps, K., Taylor, D. L. and Lanni, F., Probing the structure of cytoplasm. *J. Cell Biol.*, 1986, **102**, 2015–2022.
89. Axelrod, D., Burghardt, T. P. and Thompson, N. L., Total internal reflection fluorescence. *Annu. Rev. Biophys. Bioeng.*, 1984, **13**, 247–268.
90. Sako, Y. and Uyemura, T., Total internal reflection fluorescence microscopy for single-molecule imaging in living cells. *Cell Struct. Funct.*, 2002, **27**, 357–365.
91. Thompson, N. L., Burghardt, T. P. and Axelrod, D., Measuring surface dynamics of biomolecules by total internal reflection fluorescence with photobleaching recovery or correlation spectroscopy. *Biophys. J.*, 1981, **33**, 435–454.
92. Sund, S. E. and Axelrod, D., Actin dynamics at the living cell submembrane imaged by total internal reflection fluorescence photobleaching. *Biophys. J.*, 2000, **79**, 1655–1669.
93. Burghardt, T. P. and Axelrod, D., Total internal reflection/fluorescence photobleaching recovery study of serum albumin adsorption dynamics. *Biophys. J.*, 1981, **33**, 455–467.
94. Swaminathan, R., Bicknese, S., Periasamy, N. and Verkman, A. S., Cytoplasmic viscosity near the cell plasma membrane: translational diffusion of a small fluorescent solute measured by total internal reflection–fluorescence photobleaching recovery. *Biophys. J.*, 1996, **71**, 1140–1151.
95. Fushimi, K. and Verkman, A. S., Low viscosity in the aqueous domain of cell cytoplasm measured by picosecond polarization microfluorimetry. *J. Cell Biol.*, 1991, **112**, 719–725.
96. Verkman, A. S., Armijo, M. and Fushimi, K., Construction and evaluation of a frequency-domain epifluorescence microscope for lifetime and anisotropy decay measurements in subcellular domains. *Biophys. Chem.*, 1991, **40**, 117–125.
97. Bicknese, S., Periasamy, N., Shohet, S. B. and Verkman, A. S., Cytoplasmic viscosity near the cell plasma membrane: measurement by evanescent field frequency-domain microfluorimetry. *Biophys. J.*, 1993, **65**, 1272–1282.
98. Drake, J. M. and Klafter, J., Dynamics of confined molecular systems. *Phys. Today*, 1990, **43**, 46–55.
99. Davey, A. M., Walvick, R. P., Liu, Y., Heikal, A. A. and Sheets, E. D., Membrane order and molecular dynamics associated with IgE receptor cross-linking in mast cells. *Biophys. J.*, 2007, **92**, 343–355.
100. Pu, Y., Wang, W. B., Achilefu, S., Das, B. B., Tang, G. C., Sriramoju, V. and Alfano, R. R., Time-resolved fluorescence polarization anisotropy and optical imaging of Cybesin in cancerous and normal prostate tissues. *Opt. Commun.*, 2007, **274**, 260–267.

ACKNOWLEDGEMENT. We thank Prof. Alan S. Verkman for his comments on the article.